

Research Article

Neutral endopeptidase inhibitors blunt kidney fibrosis by reducing myofibroblast formation

© Roel Bijkerk^{1,*}, Marina A. Aleksinskaya^{1,*}, Jacques M.G.J. Duijs¹, Jennifer Veth¹, Bettina Husen², Dania Reiche², Cornelia Prehn³, Jerzy Adamski^{3,4,5}, Ton J. Rabelink¹, Jo G.R. De Mey^{6,7} and ⊚ Anton Jan van Zonneveld¹

Correspondence: A.J. van Zonneveld (a.j.vanzonneveld@lumc.nl)

Kidney fibrosis is the common pathophysiological mechanism in end-stage renal disease characterized by excessive accumulation of myofibroblast-derived extracellular matrix. Natriuretic peptides have been demonstrated to have cyclic guanosine monophosphate (cGMP)-dependent anti-fibrotic properties likely due to interference with pro-fibrotic tissue growth factor β (TGF-β) signaling. However, in vivo, natriuretic peptides are rapidly degraded by neutral endopeptidases (NEP). In a unilateral ureteral obstruction (UUO) mouse model for kidney fibrosis we assessed the anti-fibrotic effects of SOL1, an orally active compound that inhibits NEP and endothelin-converting enzyme (ECE). Mice (n=10) per group) subjected to UUO were treated for 1 week with either solvent, NEP-/ECE-inhibitor SOL1 (two doses), reference NEP-inhibitor candoxatril or the angiotensin II receptor type 1 (AT₁)-antagonist losartan. While NEP-inhibitors had no significant effect on blood pressure, they did increase urinary cGMP levels as well as endothelin-1 (ET-1) levels. Immunohistochemical staining revealed a marked decrease in renal collagen (\sim 55% reduction, P<0.05) and α -smooth muscle actin (α -SMA; \sim 40% reduction, P<0.05). Moreover, the number of α -SMA positive cells in the kidneys of SOL1-treated groups inversely correlated with cGMP levels consistent with a NEP-dependent anti-fibrotic effect. To dissect the molecular mechanisms associated with the anti-fibrotic effects of NEP inhibition, we performed a 'deep serial analysis of gene expression (Deep SAGE)' transcriptome and targeted metabolomics analysis of total kidneys of all treatment groups. Pathway analyses linked increased cGMP and ET-1 levels with decreased nuclear receptor signaling (peroxisome proliferator-activated receptor [PPAR] and liver X receptor/retinoid X receptor [LXR/RXR] signaling) and actin cytoskeleton organization. Taken together, although our transcriptome and metabolome data indicate metabolic dysregulation, our data support the therapeutic potential of NEP inhibition in the treatment of kidney fibrosis via cGMP elevation and reduced myofibroblast formation.

Received: 11 October 2018 Revised: 03 January 2019 Accepted: 06 January 2019

Accepted Manuscript Online: 07 January 2019 Version of Record published: 22 January 2019

Introduction

Chronic kidney disease (CKD) has a worldwide prevalence of 8% [1,2]. Besides its high morbidity, CKD is a leading cause of death due to premature cardiovascular disease [3]. Despite recent major improvements in the clinical management of CKD, the aging population and increasing prevalence of non-communicable diseases such as diabetes and hypertension, the numbers of CKD patients are ever increasing [4].

The ongoing decline in glomerular filtration rate in CKD patients progressively associates with kidney fibrosis and, ultimately, complete loss of kidney function and a dependence on renal replacement

¹Department of Internal Medicine (Nephrology) and the Einthoven Laboratory for Vascular and Regenerative Medicine, Leiden University Medical Center, Leiden, The Netherlands; ²Department of Medicinal Chemistry/CDS, Established Products, Abbott Products GmbH, Hannover, Germany; ³Institute of Experimental Genetics, Genome Analysis Center, Helmholtz Zentrum, Munich, Germany; ⁴German Center for Diabetes Research (DZD), München-Neuherberg, Germany; ⁵Chair for Experimental Genetics, Technical University of Munich, Freising-Weihenstephan, Germany; ⁶Department of Pharmacology, Cardiovascular Research Institute Maastricht (CARIM), Maastricht University, Maastricht, The Netherlands; ⁷Department of Physiology, Institute of Biomedicine, Aarhus University, Denmark

^{*} These authors contributed equally to this work.



therapy [3]. Kidney fibrosis is characterized by the accumulation of myofibroblasts that excessively produce and deposit extracellular matrix [3]. Targeting myofibroblast formation thus represents a promising modality to counter the development and progression of CKD. Natriuretic peptides such as C-type natriuretic peptide (CNP) were demonstrated to have cGMP-dependent anti-fibrotic properties [5–7], most likely by inhibition of tissue growth factor β (TGF- β) signaling [8,9]. However, natriuretic peptides are rapidly degraded *in vivo* by neutral endopeptidases (NEP) and; therefore, NEP inhibitors have been explored to prevent organ fibrosis [10–12].

We recently described the pharmacokinetic and pharmacodynamic properties of the novel orally active metal-loprotease inhibitor SOL1 [13]. Although designed as a combined NEP and endothelin-converting enzyme (ECE) inhibitor, *in vitro* and at neutral pH, the compound primarily appeared to be a selective NEP inhibitor. In mice, after a single subcutaneous administration (30 mg/kg) SOL1 is rapidly cleared from the circulation, but lung and particularly kidney concentrations remain significantly higher exceeding the EC₅₀ concentration for NEP inhibition for more than 24 h [13,14]. This selective accumulation may relate to the elimination of SOL1 by the kidney or to the high levels of NEP and ECE enzymes in the organ. Using the established unilateral ureteral obstruction (UUO) mouse model of kidney fibrosis we assessed the anti-fibrotic effects of the NEP/ECE inhibitor SOL1, and compared its efficacy with that of the angiotensin II receptor type 1 (AT₁)-receptor antagonist losartan and the NEP inhibitor candoxatril. In addition, transcriptomic and metabolic changes were assessed to delineate the potential mechanistic pathways involved in the observed anti-fibrotic effects.

Materials and methods

Adult male C57BL/6JRj mice (8-10 weeks old at delivery) were purchased from Janvier Labs (France). The animals were group housed n=5-6 per cage, in a temperature-controlled room (21–23°C) and maintained in a 12-h light/12-h dark cycle. Food and water were available ad libitum throughout the duration of the study. All experimental procedures were approved by and conducted in accordance with the Regulations of the Local Animal Welfare Authorities (Niedersächsisches Ministerium für Ernährung, Landwirtschaft und Verbraucherschutz, Hannover, Germany). The UUO model was performed in 12-week-old C57BL/6J mice and was achieved through a left flank incision after the mice were anesthetized by inhalation of 2-4% isoflurane, oxygen (0.8-1.5 l/min), and nitrous oxide (0.2-1.5 l/min) during the whole surgical procedure. All animals received pre- and postoperative analgesia (buprenorfine) (Temgesic, Essex Pharma, Munich, Germany): 0.05 mg/kg s.c., 30 min before start of surgery, 6 h after surgery, and 22 h after surgery. The left ureter was identified and ligated twice at the level of the lower pole of the kidney with two separate silk ties. Sham UUO was performed using the same procedures, but without ligation. Losartan (30 mg/kg) was added to the drinking water, while candoxatril (100 mg/kg) and SOL1 (30 or 100 mg/kg) were given via chow. Dosing was calculated based on usual food and water consumption, accounting for the effects of UUO slightly lowering the intake, estimated at: water and chow 2.75 g/day/animal (average 22 g). This yielded the following concentrations in water/chow: losartan (30 mg/kg body weight), 240 mg/l water; candoxatril (100 mg/kg body weight), 800mg/kg chow; SOL-1 (30 mg/kg body weight), 240 mg/kg chow; and SOL-1 (100 mg/kg body weight), 800 mg/kg chow. The compounds were homogenously mixed (grounded) into meal-chow. Blood pressure and heart rate were assessed using the CODA non-invasive tail cuff system (Kent Scientific, Torrington, CT) in conscious mice. Hematologic values were analyzed using a semi-automatic hematology analyzer (Sysmex, Corp., Etten-Leur, The Netherlands). Animals were habituated to the device before measurements. Urine creatinine concentrations were determined by the Jaffé method using 0.13% picric acid (Sigma-Aldrich, St. Louis, MO) and were quantified using a creatinine standard set (Sigma-Aldrich), as previously described [15].

Cell culture

The NIH3T3 cell line (mouse fibroblasts) was obtained from ATCC (American Type Culture Collection, Manassas, VA) and maintained in Dulbecco's modified Eagle medium (DMEM; Gibco/Invitrogen, Breda, The Netherlands) supplemented with 10% fetal calf serum (Bio Whittaker/Cambrex, Verviers, Belgium) and $1 \times L$ -glutamin (Invitrogen) with a final concentration of 2 mM. The SV40-transformed human renal fibroblast cell line TK173 has been previously characterized [16] and was maintained in DMEM supplemented with 10% fetal calf serum. TGF- β -depleted FCS was used. Cells were incubated at 37°C in 5% CO₂. Cells were treated with 2 ng/ml TGF- β 1 (R&D, Minneapolis, MN) for 48 h. CD-NP was dissolved in DMSO and added in different concentrations (0.01, 0.1, and 1 μ M) for 48 h.



Collagen assay

Cultured cells were fixed in 4% PFA for 45 min, washed with PBS, and incubated in the PicroSirius red (0.1%) staining solution at room temperature for 1 h. The staining solution was removed, and the cells were washed with PBS. HCl (0.01 N) was added for 10 min, followed by washing with PBS and subsequent elution of picroSirius red with 0,1 N NaOH for 30 min. The optical density at 550 nm was determined using a spectrophotometer.

Immunohistochemistry

Cell culture

NIH3T3 and TK173 cells were washed twice with PBS and fixed with 4% paraformaldehyde at room temperature for 5 min. The cells were subsequently washed again, and permeabilized with 0.5% Triton X-100 in PBS for 5 min at room temperature. Cells were then blocked with 10% normal goat serum in PBS for 30 min at room temperature, and incubated for 1 h with primary antibody for F-actin: 2 μ g/ml phalloidin-TRITC (Sigma–Aldrich). Immunostaining was visualized by fluorescence microscopy (Leica DM1-6000, Leica Microsystems, Rijswijk, The Netherlands).

Tissue staining

Kidneys were fixed in 10% neutral buffered formalin overnight, then dehydrated in 70% ethanol followed by paraffin embedding. Kidney sections were deparaffinized with xylene and then re-hydrated in water through graded ethanol. Sections were stained for collagen and fibrosis using Azan stain or incubated with a specific antibody against α -smooth muscle actin (α -SMA, Sigma cat. no. A2547, 1:500) and detected with ARK (DAKO Animal Research Kit, cat. no. K3954, Glostrup, Denmark) or incubated with a specific antibody against F4/80 (AbD Serotec, cat. no. 0609, 1:100, Kidlington, U.K.) and detected with Vectastain Elite ABC kit (Vector Labs, Peterborough, U.K.), followed by the appropriate secondary antibodies from those kits. Counterstaining was performed with hematoxylin. Quantification of immunohistochemistry was performed Using image J software (NIH, Bethesda, MD, U.S.A.).

The cGMP assay

The cGMP levels in urine were determined using ELISA (Cayman Chemical, Ann Arbor, MI, U.S.A.) according to the manufacturer's protocol and normalized per mol of creatinine.

RNA isolation and qPCR

Total RNA from kidneys was isolated using Trizol reagent (Invitrogen, Breda, The Netherlands). Reverse transcription was performed using a 5-min 65°C incubation of 250 ng total RNA with dNTPs (Invitrogen) and oligo (dT) (Invitrogen). cDNA was synthesized using a M-MLV First-Strand Synthesis system (Invitrogen). Validation of mRNA levels was carried out using SYBR Green Master Mix (Applied Biosystems, Bleiswijk, The Netherlands). Primer sequences of target genes are as follows: α-SMA (sense) CGTGGCTATTCCTTCGTGAC; α-SMA (antisense): GCGTTCGTAGCTCTTCTCC; collagen1α1 (Col1α1) (sense): TGACTGGAAGAGCGGAGAGT; Col1α1 (antisense): GTTCGGGCTGATGTACCAGT; β-actin (sense): AGGTCATCACTATTGGCAACGA; β-actin (antisense): CCAAGAAGGAAGGCTGGAAAA. Levels of expression were determined by normalizing to β-actin. Results were normalized using Gene Expression Analysis for iCycler IQ[®] RT-PCR Detection System (Bio-Rad Laboratories, Veenendaal, The Netherlands).

Serial analysis of gene expression

RNA was isolated from paraffin-embedded kidney tissue sections (20 μ m) using the RNeasy FFPE Kit (Qiagen, Venlo, The Netherlands) according to the manufacturer's protocol. The quality of the obtained RNA was high (RNA integrity number >9), as determined with Agilent's lab-on-chip total RNA nano assay (Agilent Technologies, Amstelveen, The Netherlands). Serial analysis of gene expression (SAGE) was performed as previously described [17,18]. In brief, SAGE libraries were prepared for each individual RNA sample with a FC-102-1005 DGE-Tag Profiling NlaIII SamplePrepKit (Illumina, Eindhoven, The Netherlands). This involves isolating RNA poly-A tails with oligo (dT) beads, converting into single and then a double-stranded cDNA, performing a first restriction digest with NlaIII (at CATG's) and retaining the 3′ most fragments, adding a 5′-linker (containing a restriction site for MmeI), performing an MmeI digestion and adding a 3′-linker. Each SAGE library was then sequenced on an individual lane on an HiSeq 2000. All tags were annotated using a database provided by Illumina.



Pathway analysis

Pathway analyses were performed using Ingenuity Pathway Analysis (IPA) software (Qiagen). Z-scores were determined with a z-score higher than 2 or lower than -2 being considered statistically significant.

Metabolomics

Targeted metabolomics measurements of kidney samples have been performed using LC-ESI-MS/MS and flow injection ESI-MS/MS analyses and the AbsoluteIDQTM p180 Kit (BIOCRATES Life Sciences AG, Innsbruck, Austria). Out of 10 µl kidney tissue homogenate, 188 metabolites can be quantified, including free carnitine, 39 acylcarnitines (Cx:y), 21 amino acids (19 proteinogenic + citrulline + ornithine), 21 biogenic amines, hexoses (sum of hexoses – about 90-95% glucose), 90 glycerophospholipids (14 lysophosphatidylcholines [lysoPC] and 76 phosphatidylcholines [PC]), and 15 sphingolipids (SMx:y). To each mg of frozen kidney tissue were added 6 μl of dry ice-cooled methanol. Frozen samples were homogenized and extracted using homogenization tubes with ceramic beads (1.4 mm) and a Precellys 24 homogenizer with an integrated cooling unit (PEQLAB Biotechnology GmbH, Germany). After centrifugation, 10 µl of the homogenate supernatant were applied to the well plate of the p180 Kit. The assay procedures of the Absolute IDQ^{TM} p180 Kit, the detailed description of the tissue preparation and the metabolite nomenclature have been described in detail previously [19,20]. Sample handling was performed by a Hamilton Microlab STARTM robot (Hamilton Bonaduz AG, Bonaduz, Switzerland) and a Ultravap nitrogen evaporator (Porvair Sciences, Leatherhead, U.K.), beside standard laboratory equipment. Mass spectrometric analyses were done on an API 4000 Triple Quadrupole System (Sciex Deutschland GmbH, Darmstadt, Germany) equipped with a 1200 Series HPLC (Agilent Technologies Deutschland GmbH, Böblingen, Germany) and a HTC PAL auto sampler (CTC Analytics, Zwingen, Switzerland) controlled by the Software Analyst 1.5.1. Data evaluation for quantification of metabolite concentrations and quality assessment were performed with the Software Analyst 1.5.1 and the MetIDQTM software package, which is an integral part of the Absolute IDQTM Kit. Internal standards were used as reference for the calculation of metabolite concentrations. The concentrations of tissue homogenates were given in µM and the concentrations of tissue samples in pmol/mg. The LOD was set to three times the values of zero samples (methanol).

Statistical analysis

All values are presented as mean with S.E.M. unless otherwise indicated. For *in vitro* experiments, a repeated measures ANOVA with Dunnett's *posthoc* test was used. For the *in vivo* experiments, one way ANOVA was used with the *posthoc* Holm–Sidak test. Correlations were analysed by Spearman's correlation method. All statistical calculations were performed using GraphPad Prism software (La Jolla, California, U.S.A.). $P \le 0.05$ was considered to denote statistical significance.

Results

CNP counteracts myofibroblast formation and increases cGMP levels in vitro

To confirm that natriuretic peptides exert anti-fibrotic effects through a cGMP-dependent mechanism [5–7], we determined whether *in vitro* stimulation of fibroblasts with CNP increases intracellular cGMP levels. To that end, we treated TGF- β -stimulated fibroblasts (both mouse NIH3T3 cells and human TK173 cells) with a stable CNP analog, CD-NP that is protected from degradation by NEPs [21]. Figure 1A demonstrates a clear TGF- β -independent increase in cGMP levels during stimulation with CD-NP with NIH3T3 responding at a dose of 0.01 and TK173 fibroblast responding at a 0.1 μ M dose. Next, we investigated the potential anti-fibrotic properties of CNP *in vitro*. As illustrated in Figure 1B–E, CD-NP-induced cGMP elevation counteracts TGF- β -induced myofibroblast formation, as evidenced by the lack of F-actin formation and the down-regulation of mRNAs for the myofibroblast markers α -SMA and Col1 α 1 and the reduction of collagen deposition by these cells (Figure 1F).

SOL1 increased urine cGMP levels in vivo

We next determined whether administration of the NEP/ECE inhibitor SOL1 also increases cGMP formation in mice and whether this is associated with decreased myofibroblast formation and kidney fibrosis. To that end, we used two doses of SOL1 (30 and 100 mg/kg) and compared the effects to those of the established NEP inhibitor candoxatril (100 mg/kg) and the AT_1 -receptor antagonist losartan (30 mg/kg) in an UUO model. Mice were treated according to the experimental setup illustrated in Figure 2A. Table 1 lists the characteristics of the mice showing uptake of the drugs and that none of the treatments affected heart rate, while blood pressure was only decreased in losartan-treated mice.



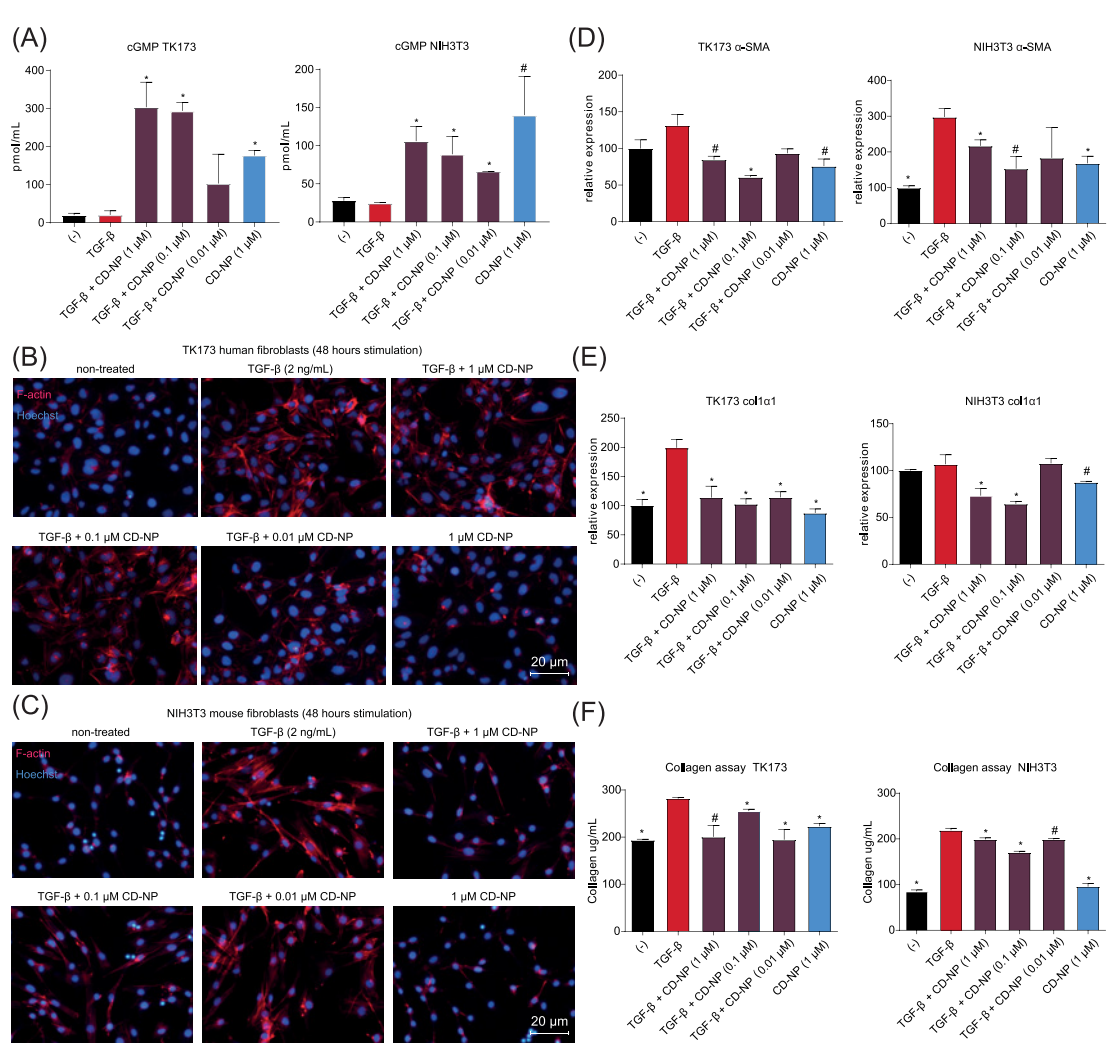


Figure 1. In vitro stimulation of fibroblasts with CD-NP increased cGMP levels and suppressed myofibroblast formation (A) Exposure of both human (TK173) and mouse (NIH3T3) TGF- β -stimulated fibroblasts to CD-NP (a stable analog of CNP) increases cGMP levels. (B,C) Representative microscopic images of F-actin staining reveals reduced myofibroblast formation by CD-NP treatment as evidenced by less F-actin formation in TK173 (B) and NIH3T3 (C) cells. (D,E) CD-NP treatment reduces α -SMA (D) and Col1 α 1 (E) gene expression in TGF- β -stimulated fibroblasts. (F) CD-NP treatment reduces Col1 α 1 production in TGF- β -stimulated fibroblasts. *P<0.05, *P<0.10, *n=4. Data are shown as mean \pm S.E.M.

Overall the hematopoietic parameters in the mice did not differ between the treatment groups apart for a minor increase of blood lymphocytes in the SOL1–100 group and a small decrease in mean cell hemoglobin level in the SOL1–30 group.

As illustrated in Figure 2B, at day 7, urinary cGMP levels dose dependently increased both in the SOL1-treated groups (SOL1–30: 200.8 \pm 30.5 mmol, P=0.12; SOL1–100: 255.1 \pm 27.3 mmol, P<0.05) and in the candoxatril group (229.4 \pm 16.1 mmol, P<0.05), compared with untreated UUO (154 \pm 11.7 mmol) and sham (146.9 \pm 14.6 mmol) mice confirming the efficacy of these compounds to raise cGMP in the kidneys of the treated animals. Given that SOL1 is a combined NEP/ECE inhibitor we also assessed endothelin-1 (ET-1) levels in the urine. Urinary ET-1 levels increased significantly during SOL1 treatment (117 \pm 45 pmol/1 in UUO versus 208 \pm 45 and 272 \pm 92 pmol/1 in the SOL1–30 and SOL1–100 groups, respectively), in contrast to what may have been expected of ECE inhibition (Table 1). This was also the case in losartan and candoxatril-treated UUO mice (Table 1).



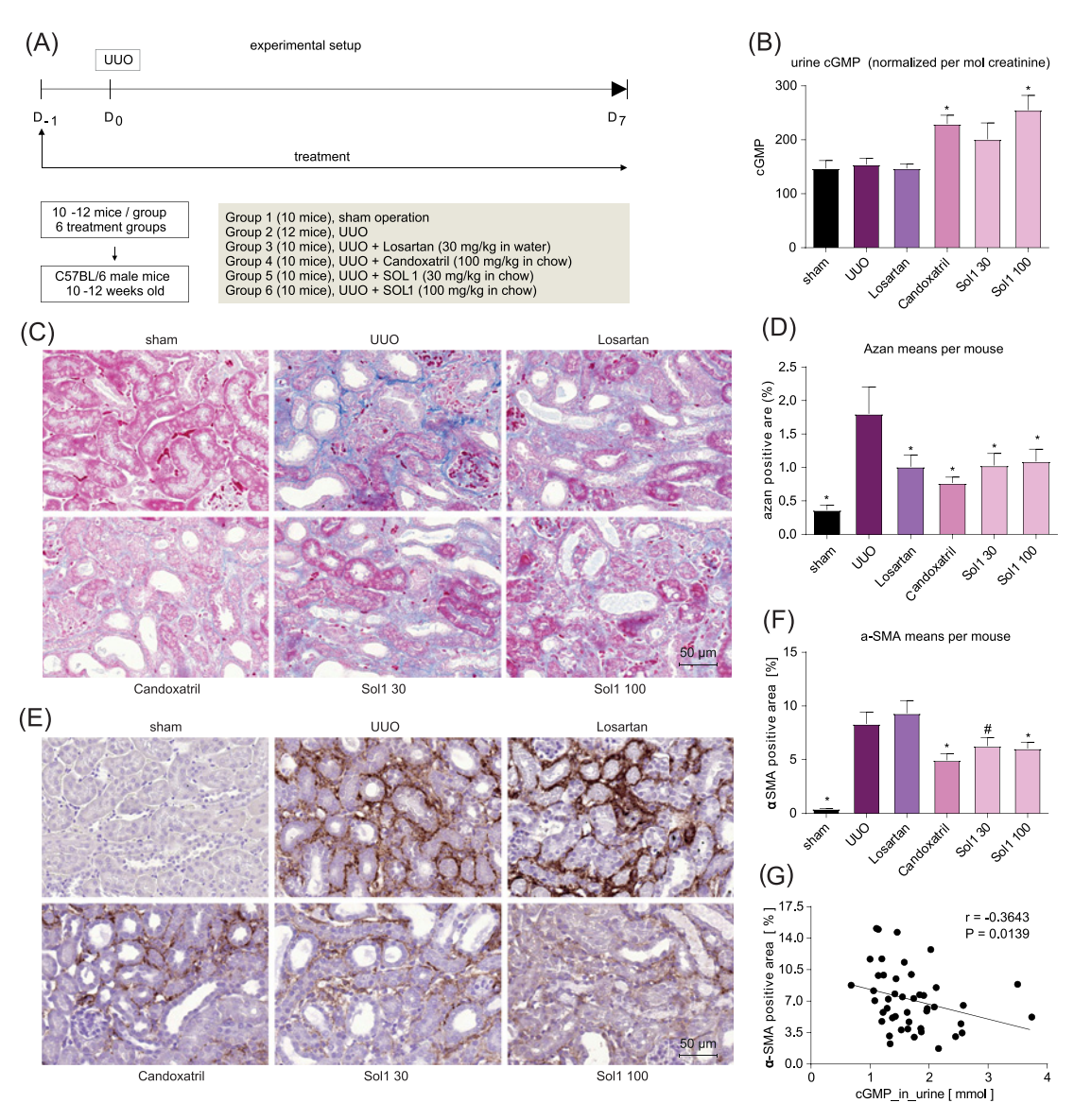


Figure 2. In vivo NEP inhibition results in decreased kidney fibrosis

(A) Experimental protocol of the *in vivo* experiment. Indicated treatments started 24 h before surgery, mice were killed 7 days after surgery. (B) Both candoxatril and SOL1 treatment resulted in increased urinary cGMP levels. (C,D) Representative microscopic images of Azan staining (C) and quantification (D) reveals decreased fibrosis (collagen deposition) in losartan, candoxatril, and SOL1-treated groups. (E,F) Representative microscopic images of α -SMA staining (E) and quantification (F) reveals decreased myofibroblast formation in candoxatril and SOL1-treated groups. (G) Inverse correlation between α -SMA positive area in the kidney and cGMP levels of SOL1-treated mice. *P <0.05, *P <0.10. Data are shown as mean + S.E.M.

NEP inhibitors SOL1 and candoxatril decrease kidney fibrosis

Given the effectiveness of the orally administrated NEP inhibitors to elevate cGMP levels in the kidneys of the treated animals we performed a detailed assessment of their anti-fibrotic properties in the unilateral obstruction model (UUO) of kidney fibrosis. As illustrated in Figure 2C,D, 7 days after UUO we observed both a dramatic increase of collagen deposition as determined by Azan staining (0.36 \pm 0.07 in sham versus 1.80 \pm 0.40 area% in UUO, P < 0.05), and a marked increase in myofibroblast formation as evidenced by increased α -SMA staining (0.41 \pm 0.04 in sham versus 8.34 \pm 1.11 area% in UUO, P < 0.05). In contrast, in mice treated with SOL1 the development of fibrosis was much less pronounced as demonstrated by significantly less collagen deposition (SOL1–30: 1.03 \pm 0.18 area%, P < 0.05; SOL1–100: 1.09 \pm 0.19 area%, P < 0.05) and myofibroblast formation (SOL1–30: 6.27 \pm 0.78 area%, P = 0.08;



Table 1 Mice characteristics

	Sham (n=10)	UUO (n=12)	UUO + Iosartan (n=10)	UUO + candoxatril (n=10)	UUO + SOL1-30 (n=10)	UUO + SOL1-100 (n=10)
Heart rate (bpm)	667 ± 69	727 ± 87	730 ± 78	699 <u>+</u> 91	697 ± 68	722 ± 54
Mean arterial blood pressure (mmHg)	96 ± 10	99 <u>+</u> 15	79 <u>+</u> 9*	102 ± 9	98 ± 10	91 <u>+</u> 13
Body weight change (g)	0.7 ± 0.8*	−0.2 ± 1	0.3 ± 0.6	1.1 ± 0.7*	1.1 ± 0.8*	-0.0 ± 0.8
Food intake (g/day)	3.3 ± 0.5	2.7 ± 0.5	2.7 ± 0.5	2.8 ± 0.4	3.1 ± 0.4	2.7 ± 0.4
Water intake (g/day)	3.2 ± 0.6	3.2 ± 1.0	2.8 ± 0.6	3.2 ± 0.8	3.3 ± 0.4	2.3 ± 1.0
ET-1 (urine, pmol/l)	158 ± 40	117 ± 45	180 ± 37*	213 ± 71*	208 ± 45*	272 ± 92*
Plasma drug level (ng/ml) – losartan	-	-	137 ± 92	-	-	-
Plasma drug level (ng/ml) – candoxatril	-	-	-	599 ± 238	-	-
Plasma drug level (ng/ml) - SOL1	-	-	-	-	45 <u>+</u> 12	172 ± 58
Weight UUO kidney (g)	0.13 ± 0.01*	0.16 ± 0.02	0.17 ± 0.02	0.15 ± 0.02	0.15 ± 0.02	0.15 ± 0.02
Weight contralateral kidney (g)	0.14 ± 0.01*	0.15 ± 0.01	0.15 ± 0.00	0.15 <u>+</u> 0.02	0.15 ± 0.01	0.15 ± 0.01
Weight hydronephrotic fluid (g)	-	0.24 ± 0.07	0.31 ± 0.03*	0.23 ± 0.05	0.22 ± 0.04	0.24 ± 0.04
White blood cells (10 ³ /μl)	6.5 ± 1.7*	11.2 ± 3.0	10.5 <u>+</u> 1.7	11.6 ± 2.9	12.1 <u>+</u> 3.2	12.8 ± 2.1
Lymphocytes (10 ³ /μl)	4.9 ±1.3*	7.7 ± 2.0	7.4 ± 1.3	7.9 ± 1.8	8.3 ± 1.9	9.5 ± 1.3*
Monocytes (10 ³ /μl)	0.2 ± 0.1*	0.4 ± 0.1	0.4 ± 0.1	0.5 ± 0.2	0.5 ± 0.2	0.5 ± 0.2
Granulocytes (103/μl)	1.4 ± 0.7*	3.1 ± 1.1	2.7 ± 0.8	3.3 ± 1.0	3.3 ± 1.7	2.9 ± 1.0
Eosinophils (%)	1.9 ± 0.9	2.4 ± 1.3	1.8 ± 0.5	3.1 ± 1.8	2.9 ± 2.8	2.2 ± 2.0
Red blood cells (10 ⁶ /μl)	10.5 ± 0.8	10.4 ± 0.7	9.7 ± 0.7	10.8 ± 0.6	10.8 ± 0.5	10.9 ± 0.7
Hemoglobin(g/dl)	14.8 ± 1.6	15.3 ± 0.7	14.4 ± 0.8*	15.8 ± 0.9	15.2 ± 1.2	15.6 ± 1.3
Hematocrit (%)	53.6 ± 4.4	52.0 ± 3.4	48.9 ± 3.6	54.2 ± 3.3	54.0 ± 3.0	54.7 ± 3.3
Mean cell volume (fl)	51.0 ± 1.0*	50.2 ± 0.6	50.2 ± 0.4	50.4 ± 0.5	50.0 ± 0.7	50.2 ± 0.8
Mean cell hemoglobin (pg)	14.2 ± 1.5	14.8 ± 0.7	14.9 ± 0.6	14.6 ± 0.3	14.0 ± 0.8*	14.3 ± 0.5
Mean cell hemoglobin concentration (g/dl)	27.8 ± 3.0	29.5 ± 1.1	29.6 ± 1.1	29.1 ± 0.7	28.1 ± 1.5*	28.5 ± 1.1*
Red cell distribution width (%)	12.9 ± 0.2	13.0 ± 0.4	13.1 ± 0.5	13.0 ± 0.3	13.1 ± 0.3	13.3 ± 0.4
Platelets (103/µl)	1291 ± 455	1741 ± 596	1960 ±583	1567 ± 543	1510 ± 706	1592 ± 884
Mean platelet volume (μm³)	5.2 ± 0.2	5.2 ± 0.3	5.1 ± 0.2	5.0 ± 0.2	5.2 ± 0.5	5.2 ± 0.3

Values are shown as mean \pm s.d. *P<0.05 compared with UUO.Abbreviation: ET-1, endothelin-1.

SOL1–100: 6.04 ± 0.59 area%, P<0.05) (Figure 2C–F). Losartan (1.01 ± 0.18 area%, P<0.05) and candoxatril (0.77 ± 0.09 area%, P<0.05) treatment resulted in a similar decrease in collagen deposition, while the NEP inhibitor candoxatril, but not losartan, also resulted in significantly decreased α -SMA levels (4.94 ± 0.61 area%, P<0.05). Moreover, α -SMA content in the kidney cortex of SOL1-treated mice was inversely correlated with urine levels of cGMP, strongly suggesting a cGMP-dependent anti-fibrotic effect (Figure 2G). While the plasma monocyte levels where not altered in the SOL1-treated mice, less macrophages were observed to accumulate in the kidneys of the treated mice compared with the control UUO kidneys (UUO: 8.01 ± 1.26 versus SOL1–30: 6.19 ± 0.89 area%, P=0.13 and SOL1–100: 4.51 ± 0.87 area%, P<0.05; Supplementary Figure S1).

Transcriptomic and metabolomic analyses

To gain insight into the molecular mechanisms underlying the anti-fibrotic effects of cGMP and ET1 elevation by the NEP inhibitors, we investigated the associated transcriptomic and metabolic changes in whole kidney samples. First, we performed a 'Deep SAGE' transcriptome analysis [17,18] in total kidney samples of all treatment groups. High



Table 2 Top 15 differentially expressed genes

Sh	Sham		Losartan		Candoxatril		SOL1-30		SOL1-100	
Ankrd13c	Fc = 2.10 P = 2.10E-13	Al316807	Fc = 1.27 P = 0,000229	Cyr61	Fc = 1.75 P = 0,000125	Rorc	Fc = 1.66 P = 4,52E-06	Sesn2	Fc = 0.70 P = 0,000732	
Dmgdh	Fc = 3.89 P = 5,35E-12	Pla2g16	Fc = 1.39 P = 0,000276	Cckar	Fc = 1.58 P = 0,00022	Dbp	Fc = 3.54 P = 1,31E-05	Enox2	Fc = 1.13 P = 0,000817	
BC014805	Fc = 5.58 P = 5,04E-11	Lrrc8d	Fc = 1.30 P = 0,000807	Cdkn1a	Fc = 0.63 P = 0,00025	Rpl18a	Fc = 1.49 P = 3,42E-05	Prosapip1	Fc = 1.34 P = 0,000828	
Wfdc2	Fc = 0.24 P = 5,3E-11	Sept11	Fc = 1.26 P = 0,000833	Angptl4	Fc = 0.56 P = 0,000597	RP23-100O18.	Fc = 1.38 1 P = 3,57E-05	Dbp	Fc = 3.26 P = 0,000873	
Agphd1	Fc = 4.12 P = 1,29E-10	Bmp4	Fc = 1.36 P = 0,000957	Scnn1g	Fc = 1.34 P = 0,000802	Rpl36al	Fc = 1.38 P = 3,78E-05	AC084109.3	Fc = 1.38 P = 0,000982	
Cfl1	Fc = 0.35 P = 4,32E-10	Rtn4ip1	Fc = 1.37 P = 0,000975	Sulf1	Fc = 0.59 P = 0,001437	AL663047.2	Fc = 1.52 P = 3,86E-05	Prdm15	Fc = 0.79 P = 0,001631	
mt-Cytb	Fc = 3.47 P = 8,59E-10	Cent1	Fc = 0.70 P = 0,000985	Edem1	Fc = 1.19 P = 0,001719	AC159636.1	Fc = 1.53 P = 4,07E-05	Ccnb2	Fc = 1.55 P = 0,001707	
Stim2	Fc = 0.47 P = 1,03E-09	March5	Fc = 1.15 P = 0,001081	Osta	Fc = 2.41 P = 0,00185	AC102483.3	Fc = 1.47 P = 5,1E-05	Cckar	Fc = 1.56 P = 0,001943	
Hibadh	Fc = 2.88 P = 1,05E-09	Dci	Fc = 1.41 P = 0,001318	Srp68	Fc = 0.85 P = 0,001985	AC122807.2	Fc = 0.80 P = 9,92E-05	Angptl4	Fc = 0.63 P = 0.003033	
Cstb	Fc = 0.24 P = 1,13E-09	Cckar	Fc = 1.53 P = 0,00197	Klhdc7a	Fc = 1.74 P = 0,002507	Xrcc4	Fc = 1.93 P = 0,000123	Rrm1	Fc = 1.26 P = 0,003177	
AU018778	Fc = 5.80 P = 1,18E-09	BC024479	Fc = 0.78 P = 0,002162	Lrrc47	Fc = 1.19 P = 0,002507	Sertad1	Fc = 1.82 P = 0,000149	Zfp697	Fc = 0.76 P = 0,003341	
Bdh1	Fc = 3.94 P = 1,18E-09	Slc5a6	Fc = 1.33 P = 0,002433	Pcdh18	Fc = 1.39 P = 0,002516	Zfp697	Fc = 0.74 P = 0,000171	Zmat5	Fc = 1.22 P = 0,003368	
Acadm	Fc = 4.46 P = 1,24E-09	Dhdds	Fc = 1.25 P = 0,002547	Map3k5	Fc = 1.23 P = 0,003069	Mtrf1I	Fc = 1.55 P = 0,000217	Pfdn5	Fc = 1.21 P = 0,003517	
St5	Fc = 0.40 P = 1,46E-09	Nudt4	Fc = 1.33 P = 0,002723	Tpcn1	Fc = 1.28 P = 0,003228	Itpkc	Fc = 1.49 P = 0,00025	S100a10	Fc = 1.47 P = 0,003729	
Mapkapk2	Fc = 0.48 P = 1,55E-09	Pdap1	Fc = 1.46 P = 0,002973	Sox12	Fc = 1.20 P = 0,003483	Thyn1	Fc1.32 P = 0,00025	Sphk2	Fc = 1.39 P = 0,004338	

SAGE analysis on RNA isolated from kidneys of different treatment groups. Fc = fold change over UUO. Top 15 differential genes (P<0.05), only genes were included with absolute levels in SAGE analysis above 10.

quality mRNA profiles were obtained from RNA isolated from 20- μ m thick sections of paraffin-embedded kidneys from at least eight independent samples per treatment group (RNA integrity [rin] values > 9).

Parallel to this transcriptomic analysis, these samples were tested for changes in targeted metabolite levels. Tables 2 and 3 summarize most differentially expressed genes and metabolites in the groups as compared with the untreated UUO group. The complete datasets can be found in Supplementary Tables S1 and S2 and in publicly available online databases. To confirm anti-fibrotic effects by SOL1, we checked the expression levels of selected fibrosis marker genes α -SMA, Col1 α 1 and connective tissue growth factor (CTGF) in our SAGE analysis and found decreased levels of these genes compared with UUO control (Figure 3A).

Pathway analysis suggests that peroxisome proliferator-activated receptor and liver X receptor/retinoid X receptor signaling and actin cytoskeleton organization are affected by NEP inhibition

With IPA, the genome wide differential gene expression data allowed for analysis of affected biological pathways associated with NEP inhibition in UUO. Figure 3B illustrates the five most affected canonical pathways for all the treatment groups (compared with UUO). Interestingly, in the SOL1 and candoxatril groups, nuclear receptor signaling, in particular peroxisome proliferator-activated receptor (PPAR) and liver X receptor/retinoid X receptor (LXR/RXR) signaling, were found to be decreased, suggesting these may be central pathways affected by NEP inhibition. Next, we assessed which canonical pathways were uniquely regulated in the NEP-inhibitor groups or SOL1 groups only, and found 16 such pathways (Figure 3C). Strikingly, most of them (six pathways) associated with actin cytoskeleton organization (cdc42 signaling, regulation of actin-based motility by Rho, actin cytoskeleton signaling, Rac signaling, signaling by RhoA family GTPases, and RhoA signaling), an important feature of myofibroblast formation and migration [22]. Likewise, when we assessed which pathways regarding 'disease and biological functions' were regulated, we observed migration and movement of cells to be markedly affected (Figure 3D), which are mainly driven by actin

Table 3 Top 15 differential metabolites

Sham Lo		Losa	Losartan Candoxatril			SOL1-30		SOL1-100		
lydroxy-valerylcarnitine (C5-OH (C3-DC-M))	fc = 2.76 p = 1,89E-13	Putrescine	Fc = 1.35 P = 0,0020	Methionine-sulfoxide(Met-SO)	Fc = 3.65 P = 6,41E-08	Methionine-sulfoxide(Met-SO)	Fc = 3.39 P = 5,54E-07	Methionine-sulfoxide(Met-SO)	Fc = 3.08 P = 4,08E-07	
PC ae C42:3	fc = 2.10 P = 9,76E-11	PC ae C44:6	Fc = 0.87 P = 0.0225	Tetradecenoyl-carnitine (C14:1)	Fc = 0.57 P = 1,53E-05	lysoPC a C24:0	Fc = 0.78 P = 2,21E-05	Hexadecenoyl-carnitine (C16:1)	Fc = 0.65 P = 0,0002	
PC aa C40:6	fc = 2.57 P = 2,10E-10	PC ae C44:4	Fc = 0.90 P = 0,0255	Hexadecenoyl-carnitine (C16:1)	Fc = 0.56 P = 2,81E-05	Acetyl-carnitine (C2)	Fc = 0.82 P = 0,0005	Hexadecanoyl-carnitine (C16)	Fc = 0.66 P = 0,0006	
PC ae C40:1	Fc = 2.27 P = 3.62E-10	PC ae C38:3	Fc = 0.90 P = 0,0346	Hydroxy-hexadecanoyl-carnitine (C16-OH)	Fc = 0.55 P = 0,0001	Hexadecenoyl-carnitine (C16:1)	Fc = 0.66 P = 0,0007	Hydroxy-hexadecenoyl-carnitine (C16:1-OH)	Fc = 0.69 P = 0,0008	
PC aa C42:4	Fc = 0.43 P = 1,71E-09	PC aa C42:0	Fc = 0.91 P = 0.0391	Dodecanoyl-carnitine(C12)	Fc = 0.69 P = 0,0002	Hydroxy-butyryl-carnitine (C3-DC (C4-OH))	Fc = 0.64 P = 0,0008	Hydroxy-tetradecenoyl-carnitine (C14:1-OH)	Fc = 0.69 P = 0,0011	
PC aa C38:5	Fc = 1.77 P = 2.11E-09			Hydroxy-hexadecenoyl-carnitine (C16:1-OH)	Fc = 0.64 P = 0,0002	Tetradecenoyl-carnitine (C14:1)	Fc = 0.73 P = 0,0009	Tetradecenoyl-carnitine (C14:1)	Fc = 0.71 P = 0.0013	
PC aa C38:6	Fc = 2.15 P = 2.81E-09			Tetradecanoyl-carnitine (C14)	Fc = 0.59 P = 0,0002	lysoPC a C26:0	Fc = 0.73 P = 0,0016	Tetradecanoyl-carnitine (C14)	Fc = 0.67 P = 0,0014	
SM C16:1	Fc = 1.87 P = 6.51E-09			Octadecenoyl-carnitine (C18:1)	Fc = 0.63 P = 0,0004	Putrescine	Fc = 1.51 P = 0,0017	Octadecenoyl-carnitine (C18:1)	Fc = 0.71 P = 0,0026	
PC ae C38:0	Fc = 1.97 P = 6,67E-09			Hexadecanoyl-carnitine (C16)	Fc = 0.63 P = 0,0004	Tetradecanoyl-carnitine (C14)	Fc = 0.67 P = 0,0019	Hydroxy-hexadecanoyl-carnitine (C16-OH)	Fc = 0.65 P = 0.0037	
PC ae C42:2	Fc = 1.78 P = 8.19E-09			Octadecanoyl-carnitine (C18)	Fc = 0.67 P = 0,0008	Hexadecanoyl-carnitine (C16)	Fc = 0.69 P = 0,0022	Putrescine	Fc = 1.42 P = 0,0044	
Carnitine (C0)	Fc = 1.98 P = 1,17E-08			Hydroxy-octadecenoyl-carnitine (C18:1-OH)	Fc = 0.67 P = 0,0008	PC ae C44:4	Fc = 0.85 P = 0,0022	Hydroxy-octadecenoyl-carnitine (C18:1-OH)	Fc = 0.72 P = 0,0060	
Creatinine	Fc = 0.11 P = 1,37E-08			Hydroxy-tetradecenoyl-carnitine (C14:1-OH)	Fc = 0.68 P = 0,0010	PC aa C42:0	Fc = 0.82 P = 0,0025	Hydroxy-tetradecadienyl-carnitine (C14:2-OH)	Fc = 0.77 • P = 0,0070	
PC ae C40:2	Fc = 1.63 P = 1,60E-08			Putrescine	Fc = 1.47 P = 0,0017	PC aa C24:0	Fc = 0.66 P = 0,0029	Hydroxy-hexadecadienyl-carnitine (C16:2-OH)	Fc = 0.81 P = 0,0105	
PC aa C34:4	Fc = 0.53 P = 3.97E-08			Hydroxy-butyryl-carnitine (C3-DC (C4-OH))	Fc = 0.69 P = 0,0024	PC aa C42:6	Fc = 0.88 P = 0,0030	Hydroxy-butyryl-carnitine (C3-DC (C4-OH))	Fc = 0.74 P = 0.0181	
PC ae C38:4	Fc = 0.64 P = 4.62E-08			Decanoyl-carnitine (C10)	Fc = 0.82 P = 0,0054	Hydroxy-tetradecenoyl-carnitine (C14:1-OH)	Fc = 0.70 P = 0,0034	PC aa C42:6	Fc = 0.92 P = 0.0197	

Targeted metabolomics analysis on kidneys of different treatment groups. Fc = fold change over UUO. Top 15 differential metabolites (P<0.05). Metabolites depicted in *italic* remain statistically significant after Bonferroni correction.







Figure 3. SAGE analysis confirms anti-fibrotic consequences of NEP-inhibition and associated pathway analyses

(A) Expression levels of fibrotic markers α -SMA, col1 α 1, and CTGF in SAGE analysis indicate decrease in fibrosis in treated groups. (B) IPA on differentially expressed genes in the SAGE datasets reveals the most affected biological pathways in the different treatment groups. Orange = increased, blue = decreased. (C–E) Comparison analysis illustrates canonical pathways (C) and diseased and biofunctions (D) and potential upstream regulators (E) that are 'specific' (enriched) for NEP-inhibitor groups (candoxatril + SOL1) or SOL1 groups only. *P <0.05, *P <0.10. Data are shown as mean \pm S.E.M.



cytoskeleton regulation [22]. Finally, we analysed upstream regulators that may control the differentially regulated genes during NEP inhibition (Figure 3E). In addition, supplementary Table 3 depicts upstream regulator analysis performed on the top 200 differentially expressed genes (P<0.05) from the SAGE analysis that are only affected in NEP inhibitor groups. These upstream regulator analyses again suggest a strong association with PPAR genes/signaling in our model.

Discussion

In this study, we demonstrated that NEP inhibition leads to increased renal cGMP levels that are associated with a decreased fibrotic phenotype of the kidneys 7 days after UUO as evidenced by a reduction in myofibroblast formation as well as a reduction in collagen deposition.

SOL1 was originally designed as an inhibitor of both NEP and ECE [13]. It was expected that its ECE inhibitory property would cause a decrease in ET-1 levels in mice, as the proteolytic processing of precursors towards active ET-1 would be inhibited. We found; however, ET-1 levels in the urine to be increased. This may be explained by the ability of NEP to degrade ET-1 [23]. Since SOL1 also inhibits NEP, our data suggest that the net effect of SOL1 treatment is less breakdown of ET-1 due to NEP inhibition than there is inhibition of ET-1 synthesis due to ECE inhibition. Consistently, it was previously demonstrated (*in vitro*) that the SOL1 compound has a higher affinity for NEP than ECE inhibition [13]. In addition, candoxatril treatment was previously demonstrated to increase ET-1 levels in patients with chronic heart failure [24]. Furthermore, ET-1 was demonstrated to promote organ fibrosis [25,26], while NEP inhibition counteracts organ fibrosis [11,12,27]. In our study, we found protection against kidney fibrosis, suggesting that the protective effects of NEP inhibition may well override the adverse effects associated with increased ET-1 levels. Consequently, our data support the notion that NEP inhibition results in increased levels of natriuretic peptides [24], yielding increased cGMP levels, that subsequently counteract the development of kidney fibrosis [5–9,28]. These results are in line with a previous study suggesting a major role for cGMP-dependent protein kinase I-α in the interstitial fibroblast [28].

Next, we aimed to delineate the potential mechanistic pathways involved in the observed anti-fibrotic effects. To that end, we performed transcriptomic and metabolomic analyses, that provided us with a comprehensive molecular signature. Using IPA, we found nuclear receptor signaling, mainly PPAR and LXR/RXR signaling, to be inhibited by dual NEP/ECE inhibition. These pathways have been extensively described to be involved in kidney fibrosis. PPAR signaling is thought to be anti-fibrotic via its inhibitory actions on TGF- β signaling [29–33]. Furthermore, RXR has been associated with increased cGMP levels [34] and has been implied in the development of renal fibrosis, also in association with PPAR signaling [32,35]. However, in our pathway analyses, we found these pathways to be down-regulated, which thus contradicts a relation to the protection against fibrosis that we observed. Although speculative, this may be explained by the increased ET-1 levels we observed, as ET-1 has been described to counteract PPAR signaling [36]. Along the same line, from the metabolomics analyses, it was striking that NEP inhibition particularly associated with decreased levels of acylcarnitines, while L-carnitine has been previously demonstrated to attenuate the development of renal fibrosis in a PPAR- γ -dependent manner [37,38]. These data further suggest an unfavourable metabolic profile around nuclear receptor signaling.

Furthermore, we found strong enrichment in the NEP inhibitor groups for signaling pathways and biological functions associated with actin cytoskeleton organization. Given that myofibroblast formation requires reorganization of the cytoskeleton resulting in the acquisition of invasive and migratory properties [22], this suggests that NEP inhibition affects the capacity of cells to transform into myofibroblasts.

Taken together, our studies identified and explored novel NEP inhibition strategies to counteract renal fibrosis and suggest that, although our transcriptomics/metabolomics analyses indicate metabolic dysregulation, therapies aimed at including NEP inhibition increase cGMP levels that stimulate anti-fibrotic signaling pathways [5–9], which may be beneficial for the treatment of CKD.

Clinical perspectives

- Natriuretic peptides have cyclic guanosine monophosphate (cGMP)-dependent anti-fibrotic properties, but in vivo, natriuretic peptides are rapidly degraded by neutral endopeptidases (NEP).
- Here, in a murine kidney fibrosis model, we demonstrated that NEP inhibitors induce cGMP levels and suppress the development of kidney fibrosis by reducing myofibroblast formation, and we determined the associated transcriptomic and metabolic changes.



 Given that renal fibrosis is the common pathophysiological mechanism in end-stage renal disease (ESRD) and is characterized by excessive accumulation of myofibroblast-derived extracellular matrix, our data suggest that NEP inhibitors deserve attention as a potential anti-fibrotic treatment to counteract the development of ESRD.

Acknowledgments

The authors thank Julia Scarpa, Werner Römisch-Margl, and Katharina Faschinger for metabolomics measurements performed at the Helmholtz Zentrum München, Genome Analysis Center, Metabolomics Core Facility. The authors thank Daniel Jasserand (Department of Medicinal Chemistry/CDS, Established Products, Abbott Products GmbH, Hannover, Germany) for his valuable advice. CD-NP was a kind gift from dr. John C. Burnett Jr. from the Mayo Clinic, Rochester, MN, USA.

Competing interests

The authors declare that there are no competing interests associated with the manuscript.

Funding

This research was performed within the framework of project T2-108 of the Dutch Top Institute Pharma. Further financial support was obtained from the Dutch Kidney Foundation (160KG16) (to R.B.) and the Dutch Heart Foundation (CVON RECONNECT).

Author contribution

A.J.v.Z., R.B., M.A.A., J.G.R.d.M., and T.J.R. designed the study. J.M.G.J.D., J.V., B.H., D.R., and C.P. carried out experiments. R.B., M.A.A., D.R., B.H., C.P., and J.A. analyzed the data and made figures. All authors drafted and/or revised the paper and approved the final version of the manuscript.

Abbreviations

 α -SMA, α -smooth muscle actin; AT₁-receptor, angiotensin II receptor type 1; cGMP, cyclic guanosine monophosphate; CKD, chronic kidney disease; CNP, C-type natriuretic peptide; Col1 α 1, collagen1 α 1; CTGF, connective tissue growth factor; DMEM, Dulbecco's modified Eagle medium; ECE, endothelin-converting enzyme; ESRD, end-stage renal disease; ET-1, endothelin-1; IPA, ingenuity pathway analysis; LXR, liver X receptor; NEP, neutral endopeptidase; PC, Phosphatidylcholine; PPAR, peroxisome proliferator-activated receptor; RXR, retinoid X receptor; SAGE, serial analysis of gene expression; TGF- β , transforming growth factor β ; UUO, unilateral ureteral obstruction.

References

- 1 Geluk, C.A., Tio, R.A., Tijssen, J.G., van Dijk, R.B., Dijk, W.A., Hillege, H.L. et al. (2007) Clinical characteristics, cardiac events and coronary angiographic findings in the prospective PREVEND cohort: an observational study. Neth. Heart J. 15, 133–141, https://doi.org/10.1007/BF03085969
- 2 Hallan, S.I., Ritz, E., Lydersen, S., Romundstad, S., Kvenild, K. and Orth, S.R. (2009) Combining GFR and albuminuria to classify CKD improves prediction of ESRD. J. Am. Soc. Nephrol. 20, 1069–1077, https://doi.org/10.1681/ASN.2008070730
- 3 Levey, A.S. and Coresh, J. (2012) Chronic kidney disease. Lancet 379, 165–180, https://doi.org/10.1016/S0140-6736(11)60178-5
- 4 National Institute of Diabetes and Digestive and Kidney Diseases: United States Renal Data System's 2010 Annual Data Report. 2010
- 5 Soeki, T., Kishimoto, I., Okumura, H., Tokudome, T., Horio, T., Mori, K. et al. (2005) C-type natriuretic peptide, a novel antifibrotic and antihypertrophic agent, prevents cardiac remodeling after myocardial infarction. *J. Am. Coll. Cardiol.* **45**, 608–616, https://doi.org/10.1016/j.jacc.2004.10.067
- 6 Murakami, S., Nagaya, N., Itoh, T., Fujii, T., Iwase, T., Hamada, K. et al. (2004) C-type natriuretic peptide attenuates bleomycin-induced pulmonary fibrosis in mice. Am. J. Physiol. Lung Cell. Mol. Physiol. 287, L1172–L1177, https://doi.org/10.1152/ajplung.00087.2004
- 7 Martin, F.L., Sangaralingham, S.J., Huntley, B.K., McKie, P.M., Ichiki, T., Chen, H.H. et al. (2012) CD-NP: a novel engineered dual guanylyl cyclase activator with anti-fibrotic actions in the heart. *PLoS ONE* 7, e52422, https://doi.org/10.1371/journal.pone.0052422
- 8 Li, P., Oparil, S., Novak, L., Cao, X., Shi, W., Lucas, J. et al. (2007) ANP signaling inhibits TGF-beta-induced Smad2 and Smad3 nuclear translocation and extracellular matrix expression in rat pulmonary arterial smooth muscle cells. *J. Appl. Physiol.* 102, 390–398, https://doi.org/10.1152/japplphysiol.00468.2006
- 9 He, J.G., Chen, Y.L., Chen, B.L., Huang, Y.Y., Yao, F.J., Chen, S.L. et al. (2010) B-type natriuretic peptide attenuates cardiac hypertrophy via the transforming growth factor-ss1/smad7 pathway in vivo and in vitro. *Clin. Exp. Pharmacol. Physiol.* 37, 283–289, https://doi.org/10.1111/j.1440-1681.2009.05281.x
- 10 Judge, P., Haynes, R., Landray, M.J. and Baigent, C. (2015) Neprilysin inhibition in chronic kidney disease. *Nephrol. Dial. Transplant.* **30**, 738–743, https://doi.org/10.1093/ndt/gfu269
- 11 Pu, Q., Amiri, F., Gannon, P. and Schiffrin, E.L. (2005) Dual angiotensin-converting enzyme/neutral endopeptidase inhibition on cardiac and renal fibrosis and inflammation in DOCA-salt hypertensive rats. *J. Hypertens.* **23**, 401–409, https://doi.org/10.1097/00004872-200502000-00023



- 12 Sharkovska, Y., Kalk, P., von Websky, K., Relle, K., Pfab, T., Alter, M. et al. (2011) Renoprotective effects of combined endothelin-converting enzyme/neutral endopeptidase inhibitor SLV338 in acute and chronic experimental renal damage. *Clin. Lab.* **57**, 507–515
- 13 Nelissen, J., Lemkens, P., Sann, H., Bindl, M., Bassissi, F., Jasserand, D. et al. (2012) Pharmacokinetic and pharmacodynamic properties of SOL1: a novel dual inhibitor of neutral endopeptidase and endothelin converting enzyme. *Life Sci.* **91**, 587–592, https://doi.org/10.1016/j.lfs.2012.01.015
- 14 Lemkens, P., Spijkers, L.J., Meens, M.J., Nelissen, J., Janssen, B., Peters, S.L. et al. (2017) Dual NEP/ECE inhibition improves endothelial function in mesenteric resistance arteries of 32-week-old SHR. *Hypertens. Res.*, https://doi.org/10.1038/hr.2017.38
- 15 Boels, M.G., Avramut, M.C., Koudijs, A., Dane, M.J., Lee, D.H., van der Vlag, J. et al. (2016) Atrasentan reduces albuminuria by restoring the glomerular endothelial glycocalyx barrier in diabetic nephropathy. *Diabetes* **65**, 2429–2439, https://doi.org/10.2337/db15-1413
- 16 Muller, G.A., Frank, J., Rodemann, H.P. and Engler-Blum, G. (1995) Human renal fibroblast cell lines (tFKIF and tNKF) are new tools to investigate pathophysiologic mechanisms of renal interstitial fibrosis. *Exp. Nephrol.* **3**, 127–133
- 17 Hestand, M.S., Klingenhoff, A., Scherf, M., Ariyurek, Y., Ramos, Y., van Workum, W. et al. (2010) Tissue-specific transcript annotation and expression profiling with complementary next-generation sequencing technologies. *Nucleic Acids Res.* **38**, e165, https://doi.org/10.1093/nar/gkq602
- 18 t Hoen, P.A., Ariyurek, Y., Thygesen, H.H., Vreugdenhil, E., Vossen, R.H., de Menezes, R.X. et al. (2008) Deep sequencing-based expression analysis shows major advances in robustness, resolution and inter-lab portability over five microarray platforms. *Nucleic Acids Res.* **36**, e141, https://doi.org/10.1093/nar/gkn705
- 19 Zukunft, S., Prehn, C., Rohring, C., Moller, G., Hrabe de Angelis, M., Adamski, J. et al. (2018) High-throughput extraction and quantification method for targeted metabolomics in murine tissues. *Metabolomics* 14, 18, https://doi.org/10.1007/s11306-017-1312-x
- 20 Zukunft S, S.M., Prehn, C., Möller, G. and Adamski, J. (2013) Targeted metabolomics of dried blood spot extracts. *Chromatographia* **76**, 1295–1305, https://doi.org/10.1007/s10337-013-2429-3
- 21 Lisy, O., Huntley, B.K., McCormick, D.J., Kurlansky, P.A. and Burnett, Jr, J.C. (2008) Design, synthesis, and actions of a novel chimeric natriuretic peptide: CD-NP. J. Am. Coll. Cardiol. 52, 60–68, https://doi.org/10.1016/j.jacc.2008.02.077
- 22 Meran, S. and Steadman, R. (2011) Fibroblasts and myofibroblasts in renal fibrosis. *Int. J. Exp. Pathol.* 92, 158–167, https://doi.org/10.1111/j.1365-2613.2011.00764.x
- 23 D'Elia, E., Iacovoni, A., Vaduganathan, M., Lorini, F.L., Perlini, S. and Senni, M. (2017) Neprilysin inhibition in heart failure: mechanisms and substrates beyond modulating natriuretic peptides. *Eur. J. Heart Fail.* **19**, 710–717, https://doi.org/10.1002/ejhf.799
- 24 McDowell, G., Coutie, W., Shaw, C., Buchanan, K.D., Struthers, A.D. and Nicholls, D.P. (1997) The effect of the neutral endopeptidase inhibitor drug, candoxatril, on circulating levels of two of the most potent vasoactive peptides. *Br. J. Clin. Pharmacol.* 43, 329–332, https://doi.org/10.1046/j.1365-2125.1997.00545.x
- 25 Ross, B., D'Orleans-Juste, P. and Giaid, A. (2010) Potential role of endothelin-1 in pulmonary fibrosis: from the bench to the clinic. *Am. J. Respir. Cell Mol. Biol.* 42, 16–20, https://doi.org/10.1165/rcmb.2009-0175TR
- 26 Widyantoro, B., Emoto, N., Nakayama, K., Anggrahini, D.W., Adiarto, S., Iwasa, N. et al. (2010) Endothelial cell-derived endothelin-1 promotes cardiac fibrosis in diabetic hearts through stimulation of endothelial-to-mesenchymal transition. *Circulation* 121, 2407–2418, https://doi.org/10.1161/CIRCULATIONAHA.110.938217
- 27 Hu, P., Xia, X., Xuan, Q., Huang, B.Y., Liu, S.Y., Zhang, D.D. et al. (2017) Neutral endopeptidase and natriuretic peptide receptors participate in the regulation of C-type natriuretic peptide expression in renal interstitial fibrosis. *J. Recept. Signal Transduct. Res.* 37, 71–83, https://doi.org/10.3109/10799893.2016.1155068
- 28 Schinner, E., Schramm, A., Kees, F., Hofmann, F. and Schlossmann, J. (2013) The cyclic GMP-dependent protein kinase lalpha suppresses kidney fibrosis. *Kidney Int.* **84**, 1198–1206, https://doi.org/10.1038/ki.2013.219
- 29 Han, S.H., Wu, M.Y., Nam, B.Y., Park, J.T., Yoo, T.H., Kang, S.W. et al. (2017) PGC-1alpha protects from Notch-induced kidney fibrosis development. *J. Am. Soc. Nephrol.* 28, 3312–3322, https://doi.org/10.1681/ASN.2017020130
- 30 Cheng, R., Ding, L., He, X., Takahashi, Y. and Ma, J.X. (2016) Interaction of PPARalpha with the canonic Wnt pathway in the regulation of renal fibrosis. *Diabetes* **65**, 3730–3743, https://doi.org/10.2337/db16-0426
- 31 Li, S., Mariappan, N., Megyesi, J., Shank, B., Kannan, K., Theus, S. et al. (2013) Proximal tubule PPARalpha attenuates renal fibrosis and inflammation caused by unilateral ureteral obstruction. *Am. J. Physiol. Renal. Physiol.* **305**, F618–F627, https://doi.org/10.1152/ajprenal.00309.2013
- 32 Kiss, E., Popovic, Z.V., Bedke, J., Adams, J., Bonrouhi, M., Babelova, A. et al. (2010) Peroxisome proliferator-activated receptor (PPAR)gamma can inhibit chronic renal allograft damage. *Am. J. Pathol.* **176**, 2150–2162, https://doi.org/10.2353/ajpath.2010.090370
- 33 Deng, Y.L., Xiong, X.Z. and Cheng, N.S. (2012) Organ fibrosis inhibited by blocking transforming growth factor-beta signaling via peroxisome proliferator-activated receptor gamma agonists. *Hepatobiliary Pancreat. Dis. Int.* **11**, 467–478, https://doi.org/10.1016/S1499-3872(12)60210-0
- 34 Wang, Y., Han, Y., Yang, J., Wang, Z., Liu, L., Wang, W. et al. (2013) Relaxant effect of all-trans-retinoic acid via N0-sGC-cGMP pathway and calcium-activated potassium channels in rat mesenteric artery. *Am. J. Physiol. Heart Circ. Physiol.* **304**, H51–H57, https://doi.org/10.1152/ajpheart.00240.2012
- 35 Gomez, I.G., MacKenna, D.A., Johnson, B.G., Kaimal, V., Roach, A.M., Ren, S. et al. (2015) Anti-microRNA-21 oligonucleotides prevent Alport nephropathy progression by stimulating metabolic pathways. *J. Clin. Invest.* **125**, 141–156, https://doi.org/10.1172/JCI75852
- 36 Wolf, D., Tseng, N., Seedorf, G., Roe, G., Abman, S.H. and Gien, J. (2014) Endothelin-1 decreases endothelial PPARgamma signaling and impairs angiogenesis after chronic intrauterine pulmonary hypertension. Am. J. Physiol. Lung Cell. Mol. Physiol. 306, L361–L371, https://doi.org/10.1152/ajplung.00277.2013
- 37 Zambrano, S., Blanca, A.J., Ruiz-Armenta, M.V., Miguel-Carrasco, J.L., Arevalo, M., Mate, A. et al. (2014) L-carnitine attenuates the development of kidney fibrosis in hypertensive rats by upregulating PPAR-gamma. *Am. J. Hypertens.* 27, 460–470, https://doi.org/10.1093/ajh/hpt268



38 Chou, H.C., Wen, L.L., Chang, C.C., Lin, C.Y., Jin, L. and Juan, S.H. (2017) L-carnitine via PPARgamma- and Sirt1-dependent mechanisms attenuates epithelial-mesenchymal transition and renal fibrosis caused by perfluorooctanesulfonate. *Toxicol. Sci. 160(2), 217-229* **160** (2), 217–229, https://doi.org/10.1093/toxsci/kfx183